ACS APPLIED MATERIALS & INTERFACES

www.acsami.org

Research Article

Plasma-Assisted Controllable Doping of Nitrogen into MoS_2 Nanosheets as Efficient Nanozymes with Enhanced Peroxidase-Like Catalysis Activity

Luping Feng, Lixiang Zhang, Sheng Zhang, Xi Chen, Pan Li, Yuan Gao, Shujing Xie, Anchao Zhang, and Hua Wang*

Cite This: *ACS Appl. Mater. Interfaces* 2020, 12, 17547−17556

Read Online

ACCESS | Metrics & More | Article Recommendations | Supporting Information

ABSTRACT: Heteroatom doping is one of the effective ways to improve the catalytic performances of nanozymes. In the present work, the plasma-assisted controllable doping of nitrogen (N) into MoS_2 nanosheets has been initially proposed, resulting in efficient nanozymes. The so-obtained nanozymes were characterized separately by TEM, XRD, XPS, and FTIR. It was discovered that the resulting N-doped MoS_2 nanosheets could present dramatically enhanced peroxidase-like catalytic activities depending on the plasma treatment time. Particularly, that with the 2-min treatment could display the highest catalytic activity, which is over 3-fold higher than that of pristine MoS_2, that was also demonstrated by the kinetics studies. Herein, the N_2 plasma treatment could facilitate the N elements to be doped covalently into MoS_2 nanosheets to achieve the increased surface wettability and affinity of nanozymes for the improved access of the electrons and substrates of catalytic reactions. More importantly, the covalent doping of N elements into MoS_2 nanosheets with a lower Fermi level, as evidenced by the DFT analysis, could facilitate the promoted electron transferring, resulting in the enhanced catalysis of N-doped MoS_2 nanozymes, in addition to the high catalytic stability in water. Such a controllable plasma treatment strategy may open a new door toward the large-scale applications for doping heteroatoms into various nanozymes with improved catalysis performances.

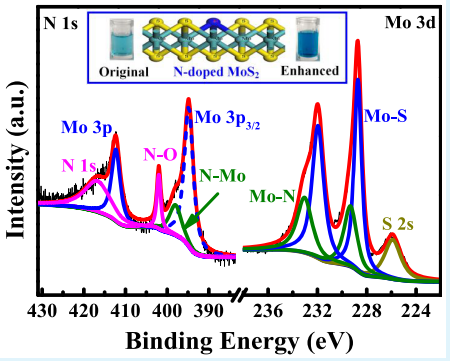

KEYWORDS: *plasma treatment, nitrogen doping, MoS_2 nanosheets, catalysis activity, nanozyme*

INTRODUCTION

Natural protein enzymes with high catalysis efficiency and substrate selectivity have been widely applied in many catalytic fields.[1,2] However, they may encounter some shortcomings such as high cost, unadjustable catalysis, and inherent instability under the external environments, which can limit their extensive applications.[3,4] Alternatively, nanozymes, as the functional nanomaterials with enzyme-like catalysis characteristics, have concentrated increasing interest due to that they can present many advantages over natural enzymes including some molecular or polymeric enzyme mimics.[5−8] Especially, in view of the low cost, tunable catalysis, multiple functionalities, and high stability against any denature or protease digestion, nanozymes have been recognized to be suitably applied in the biosensing analysis, biomedical therapeutics, catalysis, and environmental protection fields.[9−13] As representatives, the peroxidase-like nanozymes, such as nanoscaled Fe_3O_4, grapheme oxide, and MnO_2, have been preferably studied by catalyzing hydrogen peroxide (H_2O_2)-mediated reactions.[14−17]

Molybdenum disulfide (MoS_2), one of the kinds of transition-metal dichalcogenides with a two-dimensional layered structure, has been extensively applied in the fields of electronic design, catalysis, and especially biosensing and biomedicine, due to some unique advantages such as conductivity, intrinsic catalytic activity, easy surface modification, low toxicity, and high photothermal effect.[18−24] For example, Li and colleagues have applied MoS_2 as the carriers with high specific surface for loading antibodies for the sensitive immunoassays.[19] Recently, a synergetic antibacterial system was developed with polyethylene glycol-functionalized MoS_2 for effective wound disinfection by utilizing its catalytic activity and photothermal efficacy.[23] However, some shortcomings of MoS_2 such as poor dispersion in water, especially low catalytic activities, may still challenge its applications on a large scale.

It is well established that the surface properties such as wettabilities, charges, and reactive sites may generally

Received: January 30, 2020
Accepted: March 30, 2020
Published: March 30, 2020

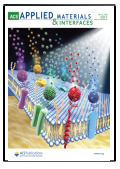

https://dx.doi.org/10.1021/acsami.0c01789
ACS Appl. Mater. Interfaces 2020, 12, 17547−17556

Scheme 1. Schematic Illustration of the Main Principle and Procedure of the Plasma Treatment for MoS_2 Nanosheets with Enhanced Peroxidase-Like Catalysis for Chromogenic TMB−H_2O_2 Reactions in Comparison with MoS_2, Where the Covalent N Doping Might Increase the Hydrophilic Wettability (Conductivity) and Create Surface Defects on MoS_2 to Promote the Electron Transferring and the Hydroxyl Radicals' Generation from Hydrogen Peroxide

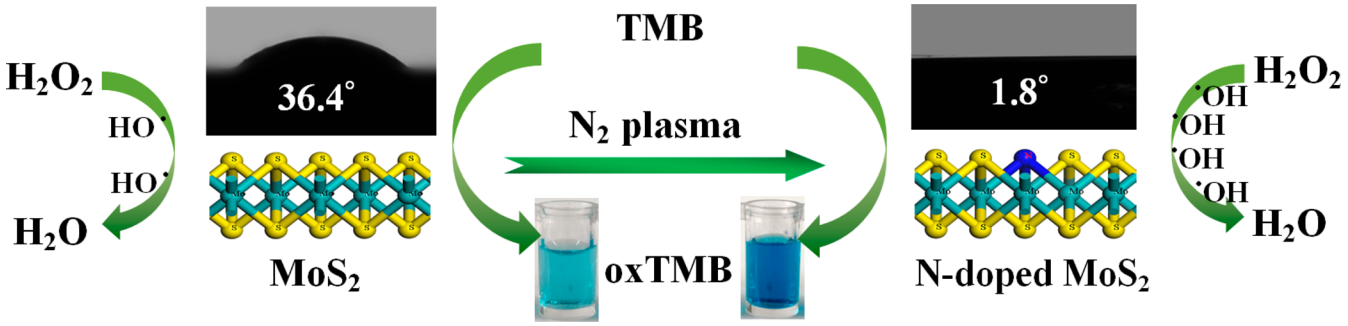

determine the catalytic performances of nanozymes such as MoS_2, although their catalysis activities can largely originate from the nanomaterials themselves.[25,26] In particular, the enhancement of aqueous dispersibility of MoS_2 can help to improve the peroxidase-like activity, catalysis velocity, and substrate affinity.[27,28] For example, Zhao and co-workers employed sodium dodecyl sulfate to modify MoS_2 to attain more efficient peroxidase-like activity for colorimetric detection of H_2O_2 and glucose.[27] Yu et al. have discovered that MoS_2 with the surface modifications of various biocompatible surfactants could exhibit surfactant-dependable catalytic performances.[28] However, the current physical modification methods, including the introduction of surfactants, might substantially bring about considerably limited improvements of catalytic capability and stability of MoS_2. Alternatively, some efforts have been devoted to the doping of various heteroatoms such as phosphorus, sulfur, and nitrogen (N) into nanozymes (such as carbon-based ones) to enhance their catalytic activities.[29−32] For example, Star's group doped N into carbon nanotube cups by chemical vapor deposition with the enhanced electrocatalysis performances for the detection of H_2O_2 and glucose.[32] Chen and colleagues have fabricated an efficient electrocatalyst by doping sulfur and N into MoO_2 nanobelts through the hydrothermal method for hydrogen evolution reactions.[31] Nevertheless, most of the current heteroatom doping methods may encounter harsh fabrication procedures such as high-temperature calcination or deposition and hydrothermal routes. Especially, the poor binding stability of doped heteroatoms in the catalytic materials may largely challenge their practical catalytic applications.

In recent years, plasma treatment technology has emerged as a simple, rapid, and highly efficient tool for the green preparation and surface modification of nanomaterials, with the merits of low energy consumption and chemical waste-free yield.[33−39] Notably, as an environmentally friendly technology, it is extremely suitable for the large-scale surface treatments or modifications of solid materials, especially two-dimensional ones, without the need of any solvent.[37−39] For example, Ji et al. demonstrated that the plasma-based surface modifications could enable the modulation of photocatalytic performances of graphitic carbon nitride.[38] Wang's group discovered that the surface properties and edge reactive sites of MoS_2 could be tuned by the plasma engineering to achieve the enhanced photocatalysis for hydrogen evolution.[39] Nevertheless, there has been no report on the improvement of peroxidase-like catalysis of nanomaterials such as MoS_2 through the plasma-assisted N doping to date.

Inspired by the pioneering works above, in the present work, MoS_2 fabricated by the hydrothermal route was treated by the N_2 plasma for N doping at room temperature, with the main procedure and principle schematically illustrated in Scheme 1. Unexpectedly, it was discovered that the resulting N-doped MoS_2 could present dramatically enhanced catalytic activities depending on the plasma treatment time, in contrast to pristine MoS_2 with an intrinsically weak catalysis. Particularly, the one with the 2-min plasma treatment could display the largest catalytic activity, which is over 3-fold higher than that of pristine MoS_2, as demonstrated by the kinetics studies. The XPS analysis results reveal that the N_2 plasma treatment could facilitate the N elements to be doped covalently into MoS_2 by forming Mo−N bonds. The increased surface wettabilities and substrate affinities of nanozymes could also be achieved for the improved access of electrons and reaction substrates. What is more, the theoretical calculations based on density functional theory (DFT) have indicated that N-doped MoS_2 could possess a lower Fermi level than the pristine MoS_2 due to that the N elements doped covalently into MoS_2 could accelerate the electron transferring of N-doped MoS_2. Furthermore, the catalytic enhancement mechanism of N-doped MoS_2 was confirmed by measuring the hydroxyl radicals ($^{\bullet}OH$) generated in the catalytic H_2O_2 oxidization-based chromogenic reactions. To the best of our knowledge, this is the first report on the improvement of peroxidase-like catalytic performances of MoS_2 nanozymes with covalent doping of heteroatoms (i.e., N) simply by the controllable plasma treatment for the catalysis applications.

EXPERIMENTAL SECTION

Reagents. Sodium molybdate dihydrate ($Na_2MoO_4{\cdot}2H_2O$) and thiourea were purchased from Sigma-Aldrich (Beijing, China). 3,3′,5,5′-Tetramethyl benzidine (TMB) and terephthalic acid (TA) were obtained from Aladdin Reagent (Shanghai, China) Co., Ltd. Acetic acid (HAc) and hydrogen peroxide (H_2O_2) were purchased from Sinopharm Chemical Reagent Co., Ltd. (Beijing, China). Deionized water (>18.2 MΩ cm) was supplied from an Ultrapure water system (Pall, U.S.). All chemicals were of analytical grade and were used as received without further purification. All of the glass containers were cleaned separately by aqua regia (*Caution: the mixture is a very corrosive oxidizing agent, which should be handled with great care*) and water before usage.

Apparatus. The N_2 plasma treatments for MoS_2 were performed using the plasma reaction system (PDC-002, Harrick, U.S.),

https://dx.doi.org/10.1021/acsami.0c01789
ACS Appl. Mater. Interfaces 2020, 12, 17547−17556

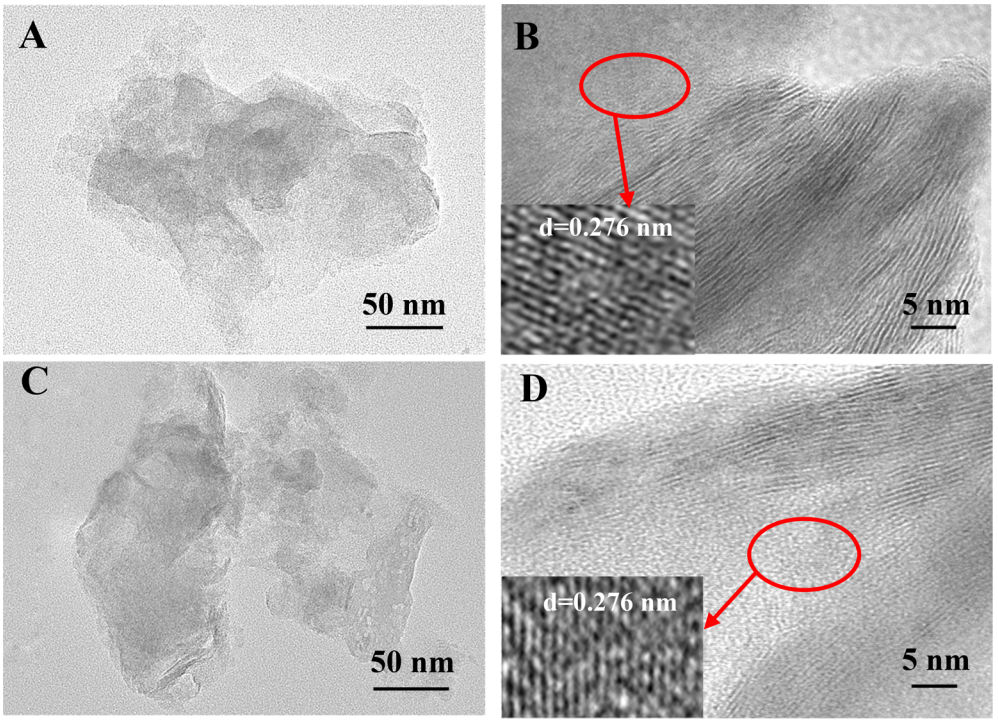

Figure 1. TEM images of (A,B) MoS_2 and (C,D) N-doped MoS_2 nanosheets with the magnitude-amplified views (inset: the sizes of the lattice fringes).

consisting of a plasma cleaner, a vacuum pump, a gas flow mixer, and a digital vacuum gauge. High-resolution transmission electron microscopy (TEM, Tecnai G20, FEI, U.S.) was employed to characterize the morphologies of the prepared MoS_2 and N-doped MoS_2. X-ray photoelectron spectroscopy (XPS, Thermo Fisher/Escalab 250xi, U.S.) was utilized for the element analysis of MoS_2 before and after the N_2 plasma treatments with a mono X-ray source. The phase compositions of the prepared materials were determined by X-ray powder diffractometer (XRD, PANalytical Model X pert3, Netherlands). The diffraction patterns of samples were recorded in the range of $2\theta = 10-80°$ using Cu Kα radiation and a fixed power source (60.0 kV, 55.0 mA). Fourier transform infrared (FTIR) spectra were recorded for MoS_2 before and after N_2 plasma treatment by using the ThermoFisher Nicolet FTIR spectrometer (Thermo Fisher, U.S.). The changing surface wettabilities of samples were monitored by measuring the contact angles (CAs) with the contact-angle measurement machine (Jinhe, Jiangsu, China). Electrical conductivities of the samples were conducted with an electrochemical workstation CHI 760D (CH Instrument, Shanghai, China) with a three-electrode system consisting of an ITO working electrode, an Ag/AgCl reference electrode, and a Pt wire counter electrode. Colorimetric measurements were performed separately using Infinite M 200 PRO (TECAN, Switzerland) with 96-well plates and a UV-3600 spectrophotometer (Shimadzu, Japan). Moreover, a table centrifuge (Thermo Scientific, Deutschland) was used in the preparation and purification procedures. The $^{\bullet}OH$ generated from H_2O_2 catalyzed by the N-doped MoS_2 and MoS_2 was determined using the fluorescence spectrophotometer (Horiba, FluoroMax-4, Japan) with a maximum fluorescence excitation wavelength of 315 nm. Besides, density functional theory (DFT) calculations were performed using the CASTEP module. The exchange-correlation interactions were described by the generalized gradient approximation with the Perdew−Burke−Ernzerh functional.

Preparation of N-Doped MoS_2. MoS_2 nanosheets were fabricated by using Na_2MoO_4 and thiourea according to a modified one-pot hydrothermal route reported previously.[40] Briefly, $Na_2MoO_4 \cdot 2H_2O$ (0.40 g) was dissolved in 30 mL of deionized water to form a clear solution by intense stirring, followed by the addition of thiourea (0.63 g) that was stirred for 20 min to form a homogeneous solution. Further, the homogeneous solution was transferred into a 50 mL Teflon-lined stainless steel autoclave to be heated at 200 °C for 24 h. After the autoclave was allowed to cool to room temperature naturally, the resulting black products were collected by centrifuging for 10 min and then washed with water and ethanol several times. Subsequently, the yielded MoS_2 nanosheets were freeze-dried for 12 h to be stored at room temperature.

The N-doped MoS_2 nanosheets were obtained by treating MoS_2 nanosheets under the plasma conditions of 13.56 MHz RF plasma at a power of 45 W and a voltage of 230 V. All of the N_2 plasma treatments were performed in the reaction chamber, into which N_2 was introduced at a flowing rate of 50 sccm, with an operating pressure kept at 100 Pa. An aliquot of MoS_2 was spread on the quartz plate in the plasma chamber to be treated for different times (2.0, 4.0, 6.0, 8.0, and 10 min) at room temperature. The so-obtained N-doped MoS_2 nanosheets were stored for the catalysis experiments.

Measurements of Peroxidase-Like Catalytic Performances. Colorimetric investigations of the peroxidase-like catalytic performances of N-doped MoS_2 nanosheets were conducted using the chromogenic TMB−H_2O_2 reactions in HAc−NaAc buffer (pH 3.6). Briefly, 5.0 mg of N-doped MoS_2 was dispersed into 1.0 mL of water under the ultrasonic conditions. An aliquot of the N-doped MoS_2 suspensions of different concentrations was added into 200 μL of TMB−H_2O_2 substrates to be incubated for 20 min at 37 °C. Furthermore, colorimetric measurements were performed for the reaction products with the absorbance values recorded. The optimization of catalytic reaction conditions was carried out with 96-well plates by following the same procedure under different reaction conditions, including different amounts of N-doped MoS_2 (20, 40, 60, 80, 100, and 120 $\mu g\ mL^{-1}$), reaction temperatures (4.0, 25, 37, 45, and 65 °C), pH values (2.0, 3.0, 4.0, 5.0, 6.0, 7.0, and 8.0), and ionic strengths in NaCl concentrations (0, 50, 100, 150, 200, 250, and 300 mM). Besides, comparable studies were conducted to explore the peroxidase-like activities of MoS_2 by the same procedure.

Studies on Michaelis−Menten Kinetics. The studies on the steady-state catalysis kinetics of N-doped MoS_2 were performed by the colorimetric tests with 96-well plates in comparison to pristine MoS_2, of which the TMB−H_2O_2 reaction substrates were used alternatively at a fixed concentration of one substrate (10 mM H_2O_2

https://dx.doi.org/10.1021/acsami.0c01789
ACS Appl. Mater. Interfaces 2020, 12, 17547−17556

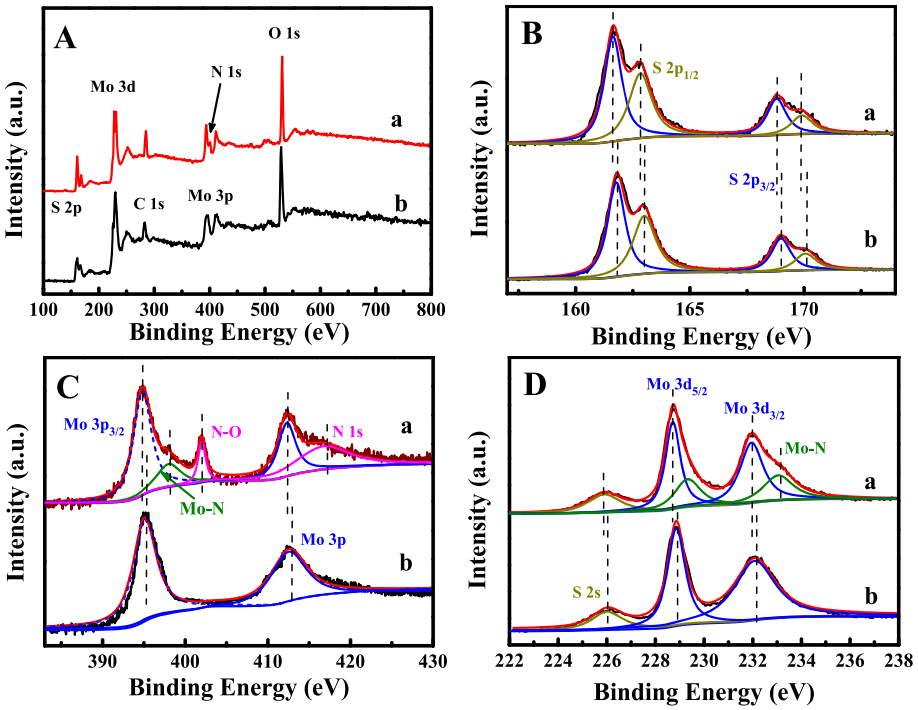

Figure 2. XPS spectra of (a) N-doped MoS_2 and (b) MoS_2 nanosheets showing the (A) survey and (B) S 2p, (C) N 1s, and (D) Mo 3d core levels.

or 800 μM TMB) and at varying concentrations of the second substrate of TMB (100, 200, 300, 400, 600, 800, and 1600 μM) or H_2O_2 (0.80, 1.60, 3.20, 6.40, and 12.8 mM). The absorbance values of the catalyzing TMB−H_2O_2 reaction products were recorded. Further, the kinetic catalysis parameters of N-doped MoS_2 and MoS_2 nanozyme were obtained by a linear-fitting method, which were calculated by the double-reciprocal plottings, including the Michaelis constant (K_m) and the maximal reaction velocity (V_{max}). Herein, the peroxidase-like affinities of N-doped MoS_2 and MoS_2 to the different reaction substrates were evaluated from the Lineweaver−Burk double-reciprocal plots derived from the Michaelis−Menten equation:

$$1/V = K_m/V_m[S] + 1/V_m$$

where V is the initial reaction velocity, V_m represents the maximal reaction velocity, [S] refers to the concentration of substrate, and K_m is the Michaelis−Menten constant.

Detection of Hydroxyl Radicals. The amounts of hydroxyl radical ($^{\bullet}$OH) generated from H_2O_2 catalyzed by N-doped MoS_2 were determined by using TA as an efficient $^{\bullet}$OH trapping agent, with the changing fluorescence intensities, taking MoS_2 nanosheets as the comparison. Briefly, an aliquot of N-doped MoS_2 was mixed immediately with H_2O_2 (1.0 mM) and TA (5.0 mM) in acetate buffer. The mixture then was stirred gently to be incubated overnight. Finally, the fluorescence intensities of the products of $^{\bullet}$OH-induced TA oxidation reactions catalyzed separately by N-doped MoS_2 and MoS_2 nanosheets were measured and compared.

RESULTS AND DISCUSSION

Preparation and Characterization of N-Doped MoS_2. MoS_2 nanosheets, which were prepared by the hydrothermal route, were controllably treated by N_2 plasma for different times at room temperature to yield the N-doped MoS_2 nanosheets. The morphologies of the obtained N-doped MoS_2 were investigated by TEM imaging, taking MoS_2 as a comparison (Figure 1). Obviously, both the N-doped MoS_2 and the MoS_2 exhibited similar morphologies (Figure 1A,B), indicating that the plasma-assisted N doping in MoS_2 might hardly destroy the morphology of MoS_2. What is more, the obtained MoS_2 materials were observed to present the nearly transparent characteristics, indicating the thin sheet structure of MoS_2, as observed elsewhere for other kinds of nanosheet materials.[41] Furthermore, Figure 1C,D shows the high-resolution TEM images of the detailed structure of the nanosheets thus developed. One can note that the interplanar spacings of about 0.27 nm, corresponding to the (100) planes of hexagonal MoS_2 nanosheets, could be clearly observed for both N-doped MoS_2 and MoS_2, which is consistent with the data reported elsewhere.[39,40]

The X-ray diffractometer (XRD) was utilized to investigate the phase structure of MoS_2 before and after N_2 plasma treatment to yield N-doped MoS_2 (Figure S1A). One can note that three kinds of diffraction peaks separately at the 2θ values of 14.52°, 32.68°, and 58.48° corresponding to the planes of (002), (100), and (110) could be obviously observed for MoS_2, which can agree well with the standard hexagonal MoS_2 (JCPDS card no. 75-1539). Importantly, the XRD pattern of N-doped MoS_2 could present similar characteristic diffraction peaks of pristine MoS_2; yet, a widened diffraction peak at the 2θ value of 32.68° could be observed, which might be ascribed to its decreased thickness.[40] Also, there are some shifts of characteristic diffraction peaks in the developed N-doped MoS_2 as compared to those of MoS_2, indicating that the N heteroatoms could be successfully doped into MoS_2 after the N_2 plasma treatment. Moreover, to explore the surface functional groups, the FTIR spectra of N-doped MoS_2 and MoS_2 were further monitored, with the results shown in Figure S2. It was found that both of the synthesized MoS_2-based nanosheets showed wide peaks at 3033 and 1635 cm^{-1}, which might be ascribed to the hydroxyl functionalities of adsorbed moisture on the surfaces. Also, three peaks located at 877, 1054, and 1212 cm^{-1} were witnessed that refer to the vibrations of the S−S and Mo−O groups. Furthermore, a characteristic peak at 455 cm^{-1} could be observed from the inset spectra, which can be assigned to the Mo−S vibration.[42]

https://dx.doi.org/10.1021/acsami.0c01789
ACS Appl. Mater. Interfaces 2020, 12, 17547−17556

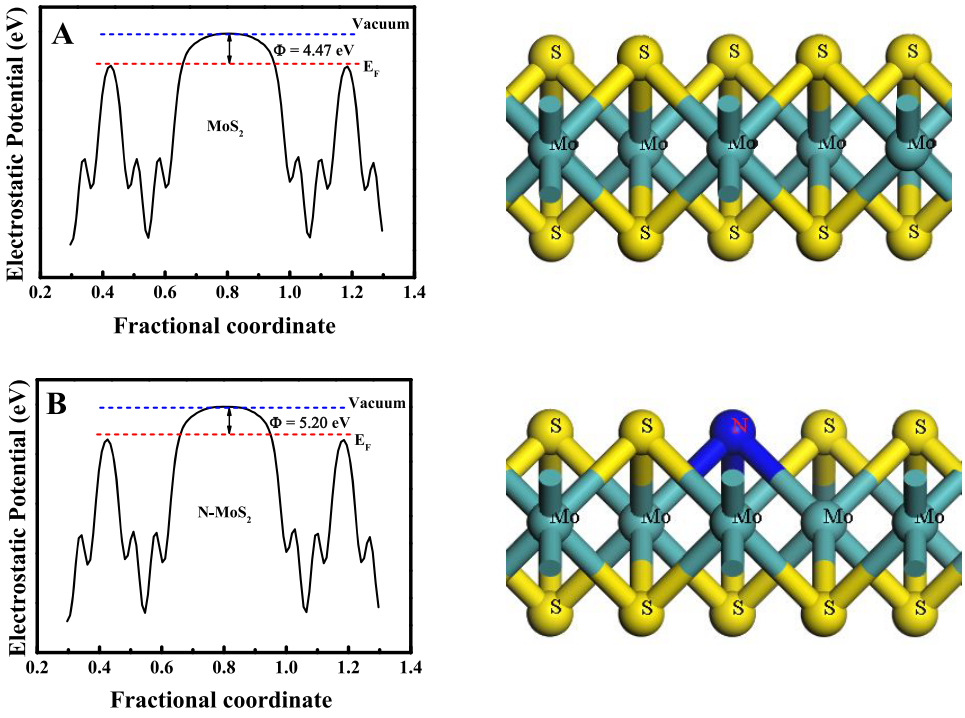

Figure 3. DFT analysis results of the optimized crystal structure, Fermi levels, and work functions of the (A) MoS_2 (001) and (B) N-doped MoS_2 nanosheets (001) calculated.

In addition, a characteristic peak at 600 cm^{-1} corresponding to the Mo−N vibration could be observed for the N-doped MoS_2,[43,44] indicating the successful doping of N elements into MoS_2 nanosheets.

The surface chemical composition and elemental valence states of the developed N-doped MoS_2 were investigated by X-ray photoelectron spectroscopy (XPS), taking MoS_2 as the comparison (Figure 2). The full scanning spectra show that the N-doped MoS_2 could present the peaks of the Mo, S, N, and O elements, in contrast to MoS_2 (Figure 2A). Herein, the O peak might come from CO_2 and O_2 adsorbed on the surfaces of materials. Moreover, Figure 2B manifests that the S 2p spectra could be obtained for both N-doped MoS_2 and MoS_2 by fitting the two $2p_{3/2}$−$2p_{1/2}$ spin−orbit doublets. It was found that four peaks located at 161.8, 162.6, 168.5, and 169.92 eV were observed. The former S 2p doublets at 161.8 and 162.6 eV can be assigned to the characteristic signals of the $2p_{3/2}$ and $2p_{1/2}$ lines in MoS_2, whereas the latter two peaks might be formed from the intermediate of thioacetamide during the hydrothermal procedure.[45] Moreover, the N 1s and Mo 3p spectra were recorded in Figure 2C, which can be deconvoluted into five peaks. Herein, the first double peaks located at 412.3 eV and the peaks located at 394.5 eV can be ascribed to the Mo 3p and Mo $3p_{3/2}$ of MoS_2, respectively. More importantly, three peaks located at 398.0, 402.0, and 417.2 eV can be separately assigned to the characteristic signals of the N−Mo bond, N−O bond, and N 1s, respectively, indicating that N elements should be covalently doped into MoS_2 nanosheets, which may aid to expect the N doping-improved stability for the N-doped nanozymes. Accordingly, the atomic percentage of N in the optimum MoS_2 nanosheets was calculated to be about 10.7 at. %. Of note, the detected characteristic signals of N−O bonds might come from O_2 adsorbed on the surface of N-doped MoS_2. Furthermore, the Mo 3d and S 2s spectra of N-doped MoS_2 were explored with the results shown in Figure 2D. Obviously, the two peaks located at around 229.0 and 232.3 eV can be assigned to the Mo 3d, which can be deconvoluted into four peaks. The first doublet peaks located at 229.0 and 232.0 eV can be assigned to the characteristic signals of Mo−S bonds, and the second ones located at 229.4 and 233.0 eV should be ascribed to the characteristic signals of Mo−N bonds.[29,46] In addition, a low intensity peak at 225.9 eV was detected in the S 2s region, which can be ascribed to the S 2s of Mo−S bonds both in MoS_2 and in N-doped MoS_2.[45,46] It is worth noting that all of the peaks of the Mo 3p, Mo 3d, S 2p, and S 2s of N-doped MoS_2 can shift negatively in comparison with those of MoS_2, suggesting the occurrence of charge transfer for N-doped MoS_2. Importantly, the Fermi level of N-doped MoS_2 might thereby move closer to the valence band of MoS_2 to allow for the easier charge transfer because of the presence of doped N as a p-type dopant, showing the band bending induced by the formation of Mo−N covalent bonds and the preferential sulfur removal, as described in the previous work.[47]

To further explore the charge transfer of the developed N-doped MoS_2, the density functional theory (DFT) calculations were comparably carried out for the Fermi levels and work functions of N-doped MoS_2 (001) and MoS_2 (001)[48] (Figure 3). One can note that the work functions of N-doped MoS_2 (001) and MoS_2 (001) can be 5.20 and 4.47 eV, respectively, revealing that the N-doped MoS_2 (001) surface might possess a lower Fermi level than that of the MoS_2 (001) surface. Considering that the band gap of N-doped MoS_2 may be assumed to be approximate to that of MoS_2,[47] a closer Fermi level to the valence band could thereby be obtained for the N-doped MoS_2, which is consistent with the XPS analysis above. The detailed energy band diagrams for the pristine MoS_2 and N-doped MoS_2 are comparably provided in Figure S3. The charge transfer could be thereby promoted toward the greatly

https://dx.doi.org/10.1021/acsami.0c01789
ACS Appl. Mater. Interfaces 2020, 12, 17547−17556

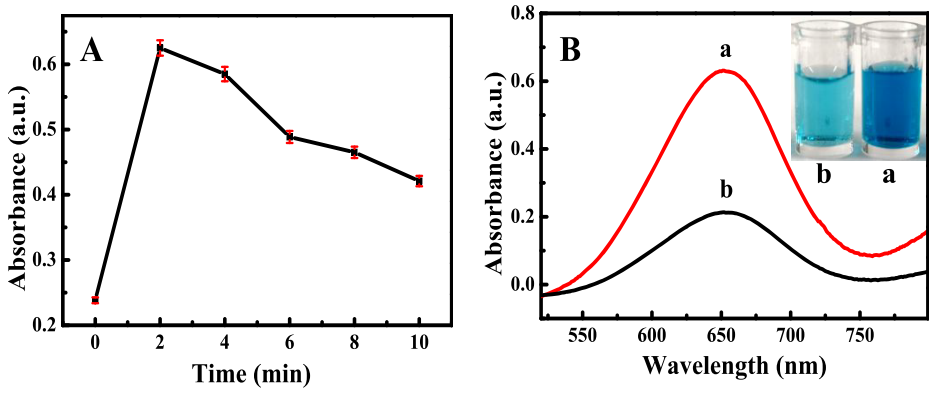

Figure 4. (A) Absorbance values of the TMB−H_2O_2 reaction solutions catalyzed by MoS_2 nanosheets treated by the nitrogen plasma for different times. (B) The UV−vis absorption spectra of TMB−H_2O_2 reaction solutions in the presence of (a) N-doped MoS_2 and (b) MoS_2 nanosheets, with the photographs of the corresponding production solutions.

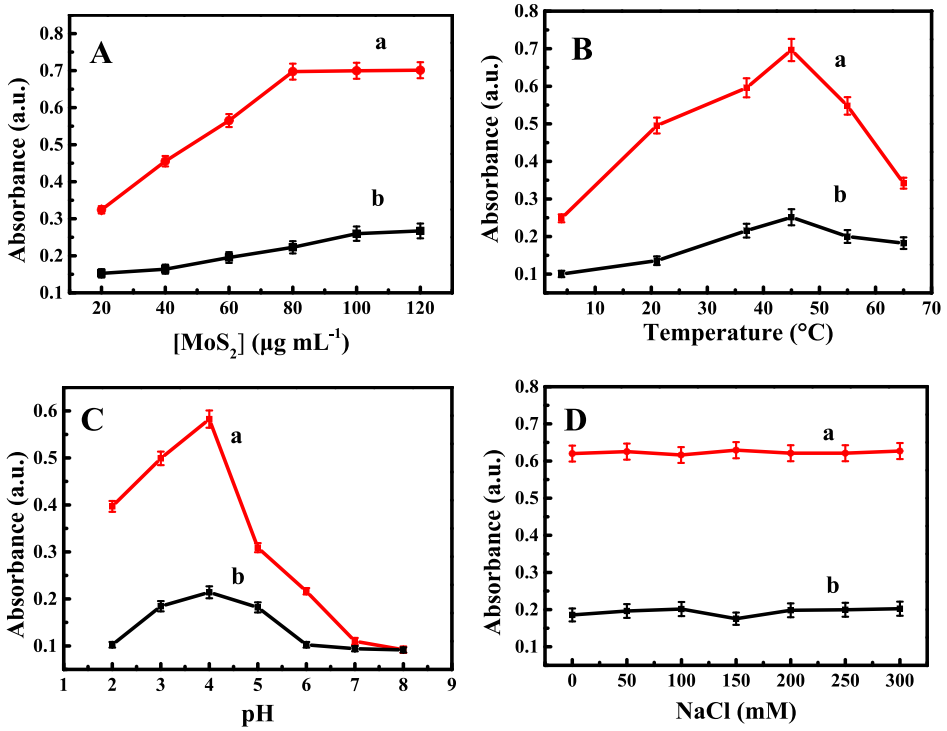

Figure 5. Optimal reaction conditions for peroxidase-like activity of (a) N-doped MoS_2 and (b) MoS_2 nanosheets, including the (A) concentration of MoS_2, (B) temperature, (C) pH values, and (D) ionic strengths in NaCl concentrations.

enhanced catalytic activities of the N-doped MoS_2 yielded by the N_2 plasma treatment, as was demonstrated after.

Plasma-Assisted Enhancement of Catalysis Performances. Scheme 1 schematically illustrates the main procedure and catalytic principle of N-doped MoS_2 formed by the plasma-assisted N doping into MoS_2 nanosheets at room temperature. As compared to the pristine MoS_2, the resulting N-doped MoS_2 could present the dramatically enhanced peroxidase-like activities in catalyzing H_2O_2 to form more hydroxyl radicals (•OH) to oxidize TMB. Moreover, the N_2 plasma treatment could significantly enhance the surface wettability of MoS_2 as evidenced in Figure S4, showing the comparison of contact angles between the N-doped MoS_2 (1.8°) and the pristine MoS_2 (36.4°).[49] Also, the enhanced affinity could be attained for the developed N-doped MoS_2, probably due to the covalent doping of N species into MoS_2 nanosheets with the increased polarity.[39] Furthermore, the electrical conductivities of N-doped MoS_2 and MoS_2 were comparably conducted by cyclic voltammetry using $K_3[Fe(CN)_6]$ (Figure S5). Apparently, the plasma-assisted N doping could additionally enhance the conductivities of MoS_2 by forming N-doped MoS_2.

The peroxidase-like catalytic activities were colorimetrically examined for the N-doped MoS_2 yielded by the N_2 plasma treatments for different time in comparison with MoS_2, where the catalytic chromogenic TMB−H_2O_2 reactions were carried out (Figure 4). As can be seen from Figure 4A, the peroxidase-like catalysis performances of N-doped MoS_2 could be enhanced with increasing the N_2 plasma treatment time to 2 min, over which time the catalytic performances would gradually decrease. Accordingly, the catalytic activities of N-doped MoS_2 can controllably depend on the treatment time,

https://dx.doi.org/10.1021/acsami.0c01789
ACS Appl. Mater. Interfaces 2020, 12, 17547−17556

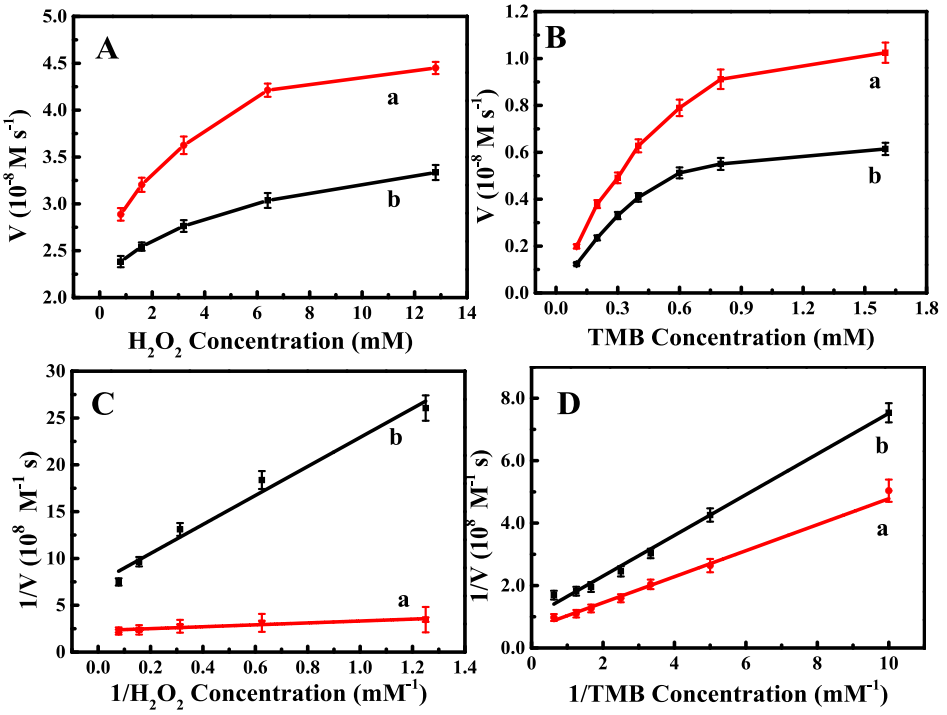

Figure 6. Comparison of catalytic dynamic data between (a) N-doped MoS_2 and (b) MoS_2 nanosheets using (A) various H_2O_2 concentrations and (B) various TMB concentrations, with (C and D) the corresponding double-reciprocal plots. The measurements were conducted alternatively at a fixed concentration of one substrate (800 μM TMB or 10 mM H_2O_2) versus varying concentrations of the second substrate, with the details shown in the experiment.

with 2 min to be selected as the optimal time for all of the catalytic experiments. More importantly, one can see from Figure 4B that a greatly enhanced peroxidase mimicking activity of N-doped MoS_2 could be quantified, as was visually witnessed by the corresponding photographs of the reaction product solutions (insert). The data are well consistent with those of the above XPS analysis and DFT calculations for N-doped MoS_2, demonstrating the enhanced peroxidase-like catalysis resulted from the N-doping-accelerated charge transfer aforementioned.

Investigation on the Peroxidase-Like Catalysis Conditions. The peroxidase-like catalysis conditions of N-doped MoS_2 and MoS_2 were comparably investigated, mainly including the nanozyme dosages, temperature, pH values, and ionic strengths in NaCl concentrations (Figure 5). It was found that both N-doped MoS_2 and MoS_2 could basically share similar optimal conditions in catalyzing the TMB–H_2O_2 reactions, including 0.080 mg mL^{-1} MoS_2 (Figure 5A), 45 °C (Figure 5B), and pH 4.0 (Figure 5C), which would be adopted as the optimized catalysis conditions for the developed nanozymes. Furthermore, Figure 5D shows that no significant effect of ionic strengths on the catalytic TMB–H_2O_2 reactions was observed for N-doped MoS_2 nanozymes, which might conduct the catalytic behavior in high salt media, even with NaCl concentrations up to 300 mM. Besides, the environmental stabilities were investigated for the developed nanozymes, which were stored over different time intervals for the catalytic tests (Figure S6). Accordingly, no significant change in catalysis performances can be expected for N-doped MoS_2 nanozymes being stored even up to 6 months, of which the high stability might be attributed to the covalently doped N in MoS_2 by the plasma treatment.

Kinetic Studies on the Peroxidase-Like Catalysis. Kinetic studies were comparably carried out on the catalytic performances of N-doped MoS_2 and pristine MoS_2 using TMB and H_2O_2 substrates, with the results shown in Figure 6, by which the Michaelis–Menten kinetics parameters were obtained. The steady-state reaction rates were first obtained by fitting the absorbance values of catalytic reaction products versus time using TMB and H_2O_2 substrates of different concentrations. Figure 6A exhibits that N-doped MoS_2 could exhibit much better peroxidase mimicking performances than pristine MoS_2 in terms of catalytic reaction rates for different H_2O_2 concentrations, which was also observed for different TMB concentrations (Figure 6B). Furthermore, the double-reciprocal plotting separately for the substrates of H_2O_2 (Figure 6C) and TMB (Figure 6D) was obtained for N-doped MoS_2 by comparison with pristine MoS_2. Accordingly, the kinetic parameters including the maximal reaction velocity (V_{max}) and Michaelis–Menten constant (K_m) were calculated in virtue of the Lineweaver–Burk plots and the Michaelis–Menten equation, with the results comparably summarized in Table 1. Accordingly, the K_m value for H_2O_2 (0.4459 mM) of

Table 1. Comparable Results of Catalysis Parameters of Dynamic Studies on the Catalysis Performances of N-Doped MoS_2 and MoS_2 Nanosheets Catalyzing the TMB–H_2O_2 Reactions

nanosheets	substrates	K_m (mM)	V_{max} (10^{-8} M s^{-1})
MoS_2	TMB	0.8246	1.161
	H_2O_2	2.0828	1.346
N-doped MoS_2	TMB	0.7916	1.796
	H_2O_2	0.4459	4.348

https://dx.doi.org/10.1021/acsami.0c01789
ACS Appl. Mater. Interfaces 2020, 12, 17547–17556

N-doped MoS_2 is much lower than that of MoS_2 (2.0828 mM), whereas they might possess the approximate K_m value for TMB, indicating the higher H_2O_2 affinities. Also, N-doped MoS_2 could present a much larger V_{max} value (4.348×10^{-8} M s^{-1}) than could pristine MoS_2 (1.346×10^{-8} M s^{-1}). The results confirm that N-doped MoS_2 should exhibit much enhanced peroxidase-like catalysis in the chromogenic TMB–H_2O_2 reactions.

Possible Catalysis Mechanism of Nanozymes. A possible mechanism is proposed for N-doped MoS_2 in catalyzing the TMB–H_2O_2 reactions through the electron transfer and hydroxyl radicals ($^{\bullet}OH$) generation processes. In the process of catalytic oxidation of TMB, herein, TMB molecules should be first absorbed on the surfaces of nanozymes and then donate the lone-pair electrons of its amino groups to MoS_2, so that the electron density and mobility of MoS_2 would be increased, as described elsewhere for other kinds of nanozyme catalysis.[15,28] Moreover, the covalently doped N components in the N-doped MoS_2 would serve as the catalytic active centers with the higher density for accelerating the electron transferring.[15,32] Also, the improved surface wettabilities and affinities could be expected for the N-doped nanozymes, so as to allow for easier access of the electrons and redox species (i.e., TMB and H_2O_2 substrates) aforementioned. Therefore, greatly accelerated electron transfer would thus be achieved for N-doped MoS_2, which can possess the lower Fermi level than that of pristine MoS_2 as verified by the DFT calculations above, which would achieve the enhanced peroxidase-like catalysis for catalyzing the decomposition of larger H_2O_2 to yield more $^{\bullet}OH$ for the oxidization of TMB.

To further confirm the proposed mechanism for the enhanced catalysis of N-doped MoS_2, the amounts of $^{\bullet}OH$ produced from H_2O_2 in the catalytic reactions were comparably monitored using terephthalic acid (TA) as an efficient $^{\bullet}OH$ trapping agent.[15,50,51] One can note from Figure S7 that the fluorescence intensities of TA-induced reaction products catalyzed by N-doped MoS_2 are much higher than that catalyzed by pristine MoS_2, suggesting that more $^{\bullet}OH$ could be effectively generated from H_2O_2 in the N-doped MoS_2-catalyzed reactions. Hence, the plasma-assisted covalent N doping should be more beneficial to $^{\bullet}OH$ radical generation, confirming the enhanced peroxidase-like catalysis of the developed N-doped MoS_2.

CONCLUSIONS

In summary, a controllable N_2 plasma treatment strategy has been applied initially for doping heteroatom N into MoS_2 nanosheets to yield the N-doped MoS_2 as efficient nanozymes. It was discovered that the resulting nanozymes could present the dramatically enhanced catalytic activities depending on the plasma treatment time. XPS analysis results reveal that the plasma treatment could facilitate the N elements to be doped covalently into MoS_2 by forming Mo–N bonds, which we expect would lead to a high catalytic stability of N-doped MoS_2 in water. Greatly increased surface wettabilities and substrate affinities of nanozymes could also be achieved to allow for the easier access of electrons and reaction substrates. Importantly, the developed N-doped MoS_2 could possess a lower Fermi level than could the pristine MoS_2 to facilitate the promoted electron transferring toward the enhanced catalysis, as evidenced by the measurements of hydroxyl radicals ($^{\bullet}OH$) generated in catalytic reactions. Besides, this simple, rapid, efficient, and controllable plasma treatment strategy can be carried out in a large-scaled way at room temperature, circumventing some limitations of the traditional modification or heteroatom doping routes under harsh conditions. Although the exact catalysis mechanism may be further explored, it may open the door toward the extensive design of different kinds of nanozymes with enhanced catalysis by the covalent doping of heteroatoms such as N and is thus promising for catalytic applications in the environmental monitoring, food safety, and biomedical analysis fields.

ASSOCIATED CONTENT

Supporting Information

The Supporting Information is available free of charge at https://pubs.acs.org/doi/10.1021/acsami.0c01789.

XRD pattern and FTIR spectra, the energy band diagrams, wettability and conductivity, and the environmental stabilities of N-doped MoS_2 and MoS_2 nanosheets; and the hydroxyl radical ($^{\bullet}OH$) amounts yielded in the catalytic reactions between N-doped MoS_2 and MoS_2 (PDF)

AUTHOR INFORMATION

Corresponding Author

Hua Wang – *School of Chemistry and Chemical Engineering and School of Environment, Harbin Institute of Technology, Harbin, Heilongjiang 150090, People's Republic of China; Institute of Medicine and Materials Applied Technologies, College of Chemistry and Chemical Engineering, Qufu Normal University, Qufu, Shandong 273165, People's Republic of China;* orcid.org/0000-0003-0728-8986; Phone: +86 537 4456306; Email: huawang@qfnu.edu.cn; http://wang.qfnu.edu.cn

Authors

Luping Feng – *School of Chemistry and Chemical Engineering, Harbin Institute of Technology, Harbin, Heilongjiang 150090, People's Republic of China*

Lixiang Zhang – *School of Environment, Harbin Institute of Technology, Harbin, Heilongjiang 150090, People's Republic of China*

Sheng Zhang – *Institute of Medicine and Materials Applied Technologies, College of Chemistry and Chemical Engineering, Qufu Normal University, Qufu, Shandong 273165, People's Republic of China*

Xi Chen – *School of Chemistry and Chemical Engineering, Harbin Institute of Technology, Harbin, Heilongjiang 150090, People's Republic of China*

Pan Li – *Institute of Medicine and Materials Applied Technologies, College of Chemistry and Chemical Engineering, Qufu Normal University, Qufu, Shandong 273165, People's Republic of China*

Yuan Gao – *Institute of Medicine and Materials Applied Technologies, College of Chemistry and Chemical Engineering, Qufu Normal University, Qufu, Shandong 273165, People's Republic of China*

Shujing Xie – *Institute of Medicine and Materials Applied Technologies, College of Chemistry and Chemical Engineering, Qufu Normal University, Qufu, Shandong 273165, People's Republic of China*

https://dx.doi.org/10.1021/acsami.0c01789
ACS Appl. Mater. Interfaces 2020, 12, 17547–17556

Anchao Zhang − *School of Mechanical and Power Engineering, Henan Polytechnic University, Jiaozuo, Henan 454000, People's Republic of China;* orcid.org/0000-0002-0704-6736

Complete contact information is available at: https://pubs.acs.org/10.1021/acsami.0c01789

Notes

The authors declare no competing financial interest.

■ ACKNOWLEDGMENTS

This study was supported by the National Natural Science Foundation of China (no. 21675099), by the Major Basic Research Program of the Natural Science Foundation of Shandong Province, People's Republic of China (ZR2018ZC0129), and by the Science and Technology Development Project of Weihai City (2015DXGJZD002), Shandong Province, People's Republic of China.

■ REFERENCES

(1) Fan, Y.; Zhang, W.; Liu, Y.; Zeng, Z.; Quan, X.; Zhao, H. Three-Dimensional Branched Crystal Carbon Nitride with Enhanced Intrinsic Peroxidase-Like Activity: A Hypersensitive Platform for Colorimetric Detection. *ACS Appl. Mater. Interfaces* **2019**, *11* (19), 17467−17474.

(2) Wiester, M. J.; Ulmann, P. A.; Mirkin, C. A. Enzyme Mimics based upon Supramolecular Coordination Chemistry. *Angew. Chem., Int. Ed.* **2011**, *50* (1), 114−137.

(3) Wang, Y.; Liu, R.; Chen, G.; Wang, L.; Yu, P.; Shu, H.; Bashir, K.; Fu, Q. Hemin-Porous gC_3N_4 Hybrid Nanosheets as an Efficient Peroxidase Mimic for Colorimetric and Visual Determination of Glucose. *Microchim. Acta* **2019**, *186* (7), 446.

(4) Wang, X.; Hu, Y.; Wei, H. Nanozymes in Bionanotechnology: From Sensing to Therapeutics and Beyond. *Inorg. Chem. Front.* **2016**, *3* (1), 41−60.

(5) Lin, T.; Zhong, L.; Wang, J.; Guo, L.; Wu, H.; Guo, Q.; Fu, F.; Chen, G. Graphite-Like Carbon Nitrides as Peroxidase Mimetics and their Applications Tto Glucose Detection. *Biosens. Bioelectron.* **2014**, *59*, 89−93.

(6) Wu, J.; Wang, X.; Wang, Q.; Lou, Z.; Li, S.; Zhu, Y.; Qin, L.; Wei, H. Nanomaterials with Enzyme-Like Characteristics (Nanozymes): Next-Generation Artificial Enzymes (II). *Chem. Soc. Rev.* **2019**, *48* (4), 1004−1076.

(7) Wang, X.; Qin, L.; Lin, M.; Xing, H.; Wei, H. Fluorescent Graphitic Carbon Nitride-Based Nanozymes with Peroxidase-Like Activities for Ratiometric Biosensing. *Anal. Chem.* **2019**, *91* (16), 10648−10656.

(8) Sun, H.; Zhou, Y.; Ren, J.; Qu, X. Carbon Nanozymes: Enzymatic Properties, Catalytic Mechanism, and Applications. *Angew. Chem., Int. Ed.* **2018**, *57* (30), 9224−9237.

(9) Duan, D.; Fan, K.; Zhang, D.; Tan, S.; Liang, M.; Liu, Y.; Zhang, J.; Zhang, P.; Liu, W.; Qiu, X. Nanozyme-Strip for Rapid Local Diagnosis of Ebola. *Biosens. Bioelectron.* **2015**, *74*, 134−141.

(10) Xu, B.; Wang, H.; Wang, W.; Gao, L.; Li, S.; Pan, X.; Wang, H.; Yang, H.; Meng, X.; Wu, Q. A Single-Atom Nanozyme for Wound Disinfection Applications. *Angew. Chem., Int. Ed.* **2019**, *58* (15), 4911−4916.

(11) Ye, H.; Yang, K.; Tao, J.; Liu, Y.; Zhang, Q.; Habibi, S.; Nie, Z.; Xia, X. An Enzyme-Free Signal Amplification Technique for Ultrasensitive Colorimetric Assay of Disease Biomarkers. *ACS Nano* **2017**, *11* (2), 2052−2059.

(12) Fan, K.; Xi, J.; Fan, L.; Wang, P.; Zhu, C.; Tang, Y.; Xu, X.; Liang, M.; Jiang, B.; Yan, X. in Vivo Guiding Nitrogen-Doped Carbon Nanozyme for Tumor Catalytic Therapy. *Nat. Commun.* **2018**, *9* (1), 1440.

(13) Zhang, Z.; Zhang, X.; Liu, B.; Liu, J. Molecular Imprinting on Inorganic Nanozymes for Hundred-Fold Enzyme Specificity. *J. Am. Chem. Soc.* **2017**, *139* (15), 5412−5419.

(14) Yin, M.; Li, S.; Wan, Y.; Feng, L.; Zhao, X.; Zhang, S.; Liu, S.; Cao, P.; Wang, H. A Selective Colorimetric Strategy for Probing Dopamine and Levodopa through the Mussel-Inspired Enhancement of Fe_3O_4 Catalysis. *Chem. Commun.* **2019**, *55* (80), 12008−12011.

(15) Song, Y.; Qu, K.; Zhao, C.; Ren, J.; Qu, X. Graphene Oxide: Intrinsic Peroxidase Catalytic Activity and its Application to Glucose Detection. *Adv. Mater.* **2010**, *22* (19), 2206−2210.

(16) Chen, J.; Meng, H.; Tian, Y.; Yang, R.; Du, D.; Li, Z.; Qu, L.; Lin, Y. Recent Advances in Functionalized MnO_2 Nanosheets for Biosensing and Biomedicine Applications. *Nanoscale Horiz.* **2019**, *4* (2), 321−338.

(17) Wei, H.; Wang, E. Fe_3O_4 Magnetic Nanoparticles as Peroxidase Mimetics and their Applications in H_2O_2 and Glucose Detection. *Anal. Chem.* **2008**, *80* (6), 2250−2254.

(18) Huang, X.; Zeng, Z.; Zhang, H. Metal Dichalcogenide Nanosheets: Preparation, Properties and Applications. *Chem. Soc. Rev.* **2013**, *42* (5), 1934−1946.

(19) Miao, L.; Zhu, C.; Jiao, L.; Li, H.; Du, D.; Lin, Y.; Wei, Q. Smart Drug Delivery System-Inspired Enzyme-Linked Immunosorbent Assay based on Fluorescence Resonance Energy Transfer and Allochroic Effect Induced Dual-Modal Colorimetric and Fluorescent Detection. *Anal. Chem.* **2018**, *90* (3), 1976−1982.

(20) Lukowski, M. A.; Daniel, A. S.; Meng, F.; Forticaux, A.; Li, L.; Jin, S. Enhanced Hydrogen Evolution Catalysis from Chemically Exfoliated Metallic MoS_2 Nanosheets. *J. Am. Chem. Soc.* **2013**, *135* (28), 10274−10277.

(21) Zhu, C.; Du, D.; Lin, Y. Graphene-Like 2D Nanomaterial-Based Biointerfaces for Biosensing Applications. *Biosens. Bioelectron.* **2017**, *89*, 43−55.

(22) Kalantar-zadeh, K.; Ou, J. Z. Biosensors based on Two-Dimensional MoS_2. *ACS Sensors* **2016**, *1* (1), 5−16.

(23) Zhu, X.; Ji, X.; Kong, N.; Chen, Y.; Mahmoudi, M.; Xu, X.; Ding, L.; Tao, W.; Cai, T.; Li, Y. Intracellular Mechanistic Understanding of 2D MoS_2 Nanosheets for Anti-Exocytosis-Enhanced Synergistic Cancer Therapy. *ACS Nano* **2018**, *12* (3), 2922−2938.

(24) Tan, C.; Cao, X.; Wu, X.; He, Q.; Yang, J.; Zhang, X.; Chen, J.; Zhao, W.; Han, S.; Nam, G. H. Recent Advances in Ultrathin Two-Dimensional Nanomaterials. *Chem. Rev.* **2017**, *117* (9), 6225−6331.

(25) Liu, B.; Liu, J. Surface Modification of Nanozymes. *Nano Res.* **2017**, *10* (4), 1125−1148.

(26) Zhou, W.; Zhou, K.; Hou, D.; Liu, X.; Li, G.; Sang, Y.; Liu, H.; Li, L.; Chen, S. Three-Dimensional Hierarchical Frameworks based on MoS_2 Nanosheets Self-Assembled on Graphene Oxide for Efficient Electrocatalytic Hydrogen Evolution. *ACS Appl. Mater. Interfaces* **2014**, *6* (23), 21534−21540.

(27) Zhao, K.; Gu, W.; Zheng, S.; Zhang, C.; Xian, Y. SDS-MoS_2 Nanoparticles as Highly-Efficient Peroxidase Mimetics for Colorimetric Detection of H_2O_2 and Glucose. *Talanta* **2015**, *141*, 47−52.

(28) Yu, J.; Ma, D.; Mei, L.; Gao, Q.; Yin, W.; Zhang, X.; Yan, L.; Gu, Z.; Ma, X.; Zhao, Y. Peroxidase-Like Activity of MoS_2 Nanoflakes with Different Modifications and their Application for H_2O_2 and Glucose Detection. *J. Mater. Chem. B* **2018**, *6* (3), 487−498.

(29) Lv, K.; Suo, W.; Shao, M.; Zhu, Y.; Wang, X.; Feng, J.; Fang, M. Nitrogen Doped MoS_2 and Nitrogen Doped Carbon Dots Composite Catalyst for Electroreduction CO_2 to CO with High Faradaic Efficiency. *Nano Energy* **2019**, *63*, 103834.

(30) Pang, L.; Barras, A.; Zhang, Y.; Amin, M. A.; Addad, A.; Szunerits, S.; Boukherroub, R. CoO Promoted the Catalytic Activity of Nitrogen-Doped MoS_2 Supported on Carbon Fibers for Overall Water Splitting. *ACS Appl. Mater. Interfaces* **2019**, *11* (35), 31889−31898.

(31) Zhou, W.; Hou, D.; Sang, Y.; Yao, S.; Zhou, J.; Li, G.; Li, L.; Liu, H.; Chen, S. MoO_2 Nanobelts@Nitrogen Self-Doped MoS_2 Nanosheets as Effective Electrocatalysts for Hydrogen Evolution Reaction. *J. Mater. Chem. A* **2014**, *2* (29), 11358−11364.

(32) Tang, Y.; Allen, B. L.; Kauffman, D. R.; Star, A. Electrocatalytic Activity of Nitrogen-Doped Carbon Nanotube Cups. *J. Am. Chem. Soc.* **2009**, *131* (37), 13200−13201.

(33) Dou, S.; Tao, L.; Wang, R.; El Hankari, S.; Chen, R.; Wang, S. Plasma-Assisted Synthesis and Surface Modification of Electrode Materials for Renewable Energy. *Adv. Mater.* **2018**, *30* (21), 1705850.
(34) Chen, Y.; Wang, H.; Liu, C.; Zeng, Z.; Zhang, H.; Zhou, C.; Jia, X.; Yang, Y. Formation of Monometallic Au and Pd and Bimetallic Au-Pd Nanoparticles Confined in Mesopores via Ar Glow-Discharge Plasma Reduction and their Catalytic Applications in Aerobic Oxidation of Benzyl Alcohol. *J. Catal.* **2012**, *289*, 105−117.
(35) Yu, X.; Zhang, F.; Wang, N.; Hao, S.; Chu, W. Plasma-Treated Bimetallic Ni-Pt Catalysts Derived from Hydrotalcites for the Carbon Dioxide Reforming of Methane. *Catal. Lett.* **2014**, *144* (2), 293−300.
(36) Gu, W.; Hu, L.; Zhu, X.; Shang, C.; Li, J.; Wang, E. Rapid Synthesis of Co_3O_4 Nanosheet Arrays on Ni Foam by in Situ Electrochemical Oxidization of Air-Plasma Engraved $Co(OH)_2$ for Efficient Oxygen Evolution. *Chem. Commun.* **2018**, *54* (90), 12698−12701.
(37) Chevallier, P.; Castonguay, M.; Turgeon, S.; Dubrulle, N.; Mantovani, D.; McBreen, P.; Wittmann, J.; Laroche, G. Ammonia RF-Plasma on PTFE Surfaces: Chemical Characterization of the Species Created on the Surface by Vapor-Phase Chemical Derivatization. *J. Phys. Chem. B* **2001**, *105* (50), 12490−12497.
(38) Ji, X.; Yuan, X.; Wu, J.; Yu, L.; Guo, H.; Wang, H.; Zhang, H.; Yu, D.; Zhao, Y. Tuning the Photocatalytic Activity of Graphitic Carbon Nitride by Plasma-Based Surface Modification. *ACS Appl. Mater. Interfaces* **2017**, *9* (29), 24616−24624.
(39) Tao, L.; Duan, X.; Wang, C.; Duan, X.; Wang, S. Plasma-Engineered MoS_2 Thin-Film as an Efficient Electrocatalyst for Hydrogen Evolution Reaction. *Chem. Commun.* **2015**, *51* (35), 7470−7473.
(40) Sun, S.; Li, X.; Wang, W.; Zhang, L.; Sun, X. Photocatalytic Robust Solar Energy Reduction of Dinitrogen to Ammonia on Ultrathin MoS_2. *Appl. Catal., B* **2017**, *200*, 323−329.
(41) Wu, C.; Lu, X.; Peng, L.; Xu, K.; Xu, P.; Huang, J.; Yu, G.; Xie, Y. Two-dimensional vanadyl phosphate ultrathin nanosheets for high energy density and flexible pseudocapacitors. *Nat. Commun.* **2018**, *4*, 2431.
(42) Massey, A. T.; Gusain, R.; Kumari, S.; Khatri, O. P. Hierarchical Microspheres of MoS_2 Nanosheets: Efficient and Regenerative Adsorbent for Removal of Water-Soluble Dyes. *Ind. Eng. Chem. Res.* **2016**, *55* (26), 7124−7131.
(43) Liu, H.; Wang, B.; Li, D.; Zeng, X.; Tang, X.; Gao, Q.; Cai, J.; Cai, H. MoS_2 Nanosheets with Peroxidase Mimicking Activity as Viable Dual-Mode Optical Probes for Determination and Imaging of Intracellular Hydrogen Peroxide. *Microchim. Acta* **2018**, *185* (6), 287.
(44) Hector, A. L.; Parkin, I. P. Sodium Azide as a Reagent for Solid State Metathesis Preparations of Refractory Metal Nitrides. *Polyhedron* **1995**, *14* (7), 913−917.
(45) Wang, Y.; Ni, Y. Molybdenum Disulfide Quantum Dots as a Photoluminescence Sensing Platform for 2, 4, 6-Trinitrophenol Detection. *Anal. Chem.* **2014**, *86* (15), 7463−7470.
(46) Koroteev, V.; Bulusheva, L.; Asanov, I.; Shlyakhova, E.; Vyalikh, D.; Okotrub, A. Charge Transfer in the MoS_2/Carbon Nanotube Composite. *J. Phys. Chem. C* **2011**, *115* (43), 21199−21204.
(47) Azcatl, A.; Qin, X.; Prakash, A.; Zhang, C.; Cheng, L.; Wang, Q.; Lu, N.; Kim, M. J.; Kim, J.; Cho, K. Covalent Nitrogen Doping and Compressive Strain in MoS_2 by Remote N_2 Plasma Exposure. *Nano Lett.* **2016**, *16* (9), 5437−5443.
(48) Zhang, L.; Li, P.; Feng, L.; Chen, X.; Jiang, J.; Zhang, S.; Zhang, C.; Zhang, A.; Chen, G.; Wang, H. Synergetic Ag_2S and ZnS quantum dots as the sensitizer and recognition probe: A visible light-driven photoelectrochemical sensor for the ″signal-on″ analysis of mercury (II). *J. Hazard. Mater.* **2020**, *387*, 121715.
(49) Feng, L.; Liu, M.; Liu, H.; Fan, C.; Cai, Y.; Chen, L.; Zhao, M.; Chu, S.; Wang, H. High-Throughput and Sensitive Fluorimetric Strategy for MicroRNAs in Blood Using Wettable Microwells Array and Silver Nanoclusters with Red Fluorescence Enhanced by Metal Organic Frameworks. *ACS Appl. Mater. Interfaces* **2018**, *10* (28), 23647−23656.
(50) Xi, Z.; Cheng, X.; Gao, Z.; Wang, M.; Cai, T.; Muzzio, M.; Davidson, E.; Chen, O.; Jung, Y.; Sun, S. Strain Effect in Palladium Nanostructures as Nanozymes. *Nano Lett.* **2020**, *20* (1), 272−277.
(51) Plauck, A.; Stangland, E. E.; Dumesic, J. A.; Mavrikakis, M. Active Sites and Mechanisms for H_2O_2 Decomposition Over Pd Catalysts. *Proc. Natl. Acad. Sci. U. S. A.* **2016**, *113* (14), E1973−E1982.

https://dx.doi.org/10.1021/acsami.0c01789
ACS Appl. Mater. Interfaces 2020, 12, 17547−17556